NASA-TM-75899 19810013491

NASA TECHNICAL MEMORANDUM

NASA TM-75899

THREE-DIMENSIONAL SEPARATED FLOWS PAST GROUND VEHICLES

F. Chometon and P. Fontanet

Translation of "Ecoulements tridimensionnels décollés autour de véhicules terrestres", Association Aéronautique et Astronautique de France, Colloque d'Aerodynamique Appliquée, 16th, Lille, France, Nov. 13-15, 1979, Paper NT 80-23, pp 1-31.

NATIONAL AERONAUTICS AND SPACE ADMINISTRATION
WASHINGTON, D.C. 20546 MAY 1981

STANDARD TITLE PAGE

1. Report No. NASA TM- 75899	2. Government Accession No.	3. Recipient's Catalog No.
4. Title and Subtitle: THREE DIMENSIONAL SEPARATED FLOWS PAST GROUND VEHICLES		5. Report Date May, 1981 6. Performing Organization Code
7. Author(s) F. Chometon (Conservatoire National des Arts et Métiers, Paris) and P. Fontanet (Régie Nationale des Usines Renault, Boulogne-Billancourt, France)		8. Performing Organization Report No. 10. Work Unit No. 11. Contract or Grant No. NASW-3199
9. Performing Organization Name and Address Leo Kanner Associates Redwood City, California 94063		13. Type of Report and Period Covered Translation
12. Sponsoring Agency Name and Address National Aeronautics and Space Administration, Washington, D.C. 20546		14. Sponsoring Agency Code

15. Supplementary Notes
Translation of "Ecoulements tridimensionnels décollés autour de véhicules terrestres", Association Aéronautique et Astronautique de France, Colloque d'Aerodynamique Appliquée, 16th, Lille, France, Nov. 13-15, 1979, Paper NT 80-23, pp 1-31.

16. Abstract

The separated flow past a thick body is calculated using a theoretical model based on a discrete wake-vortex representation. Rehbach's unsteady inviscid scheme (1977) has been used in the three-dimensional analysis. The obstacle is represented by singularities, and the wake is modeled by vortex particles emitted at the separation line. Calculated results for an axisymmetric body are compared with flow visualization results. N.D.

17. Key Words (Selected by Author(s))	18. Distribution Statement
	Unclassified - Unlimited

19. Security Classif. (of this report)	20. Security Classif. (of this page)	21. No. of Pages	22. Price
Unclassified	Unclassified	34	

Three-Dimensional Separated Flows past Ground Vehicles

F. Chometon
Conservatoire National des Arts et Métiers, Paris, France

P. Fontanet
Régie Nationale des Usines Renault, Boulogne-Billancourt, Hauts-de-Seine, France

We wish to thank the personnel of the OAT Agency of ONERA, and particularly Mr. C. Rehbach, for their generous help.

Introduction

A method for calculating three dimensional separated flow around bodies similar to ground vehicles was investigated in collaboration with the Office National d'Etudes et de Recherches Aérospatiales in Châtillon. This investigation was a continuation of research started in 1975 in which we have analyzed many results obtained in wind and water tunnels and proposed [15] a two dimensional approach based on a wake-vortex representation.

In the present article the investigation has been extended to three dimensions, and a nonstationary, inviscid scheme based on the method developed by Rehbach [1] is proposed.

The obstacle is represented by singularities and the wake is modeled with the aid of vortex particles emitted from the separation line, which is assumed to be known in this case.

The calculations carried out for axisymmetric bodies show the evolution of the vortex sheet's structure as a function of the angle of the flat base area. Wind tunnel visualizations confirmed the results. The sheet, which is of a separated two dimensional nature for an upright base area, takes on a split sheet structure for greatly inclined base areas [8], with lateral rollup present.

The numerical results presented constitute a first approximation of the problem. They especially show the necessity of an in-depth study of three dimensional separation.

Chapter 1 -- The Physical Problem /1.1*

1.1 Introduction

A physical analysis of the base area flow past simple bodies related to ground vehicles was conducted in the Lelarge-Renault wind tunnel at the Institut Aérotechnique at Saint-Cyr-l'Ecole. The experiments' main goal was to complete the recent information obtained by other authors. (Morel, Maull [2] in 1976)

The body investigated (figure 1.1) was composed of a common forward part made up of a Rankine half-body [3] with a diameter $\emptyset$ = 160 mm and length L = 700 mm. Fitted to it are flat base areas with angles α = 0°, 30°, and 60°. The assembly is mounted at zero incidence and sideslip with aid of streamlined supports. Height H can take on two values: $H/\emptyset$ = 2 and $H/\emptyset$ = 0.65.

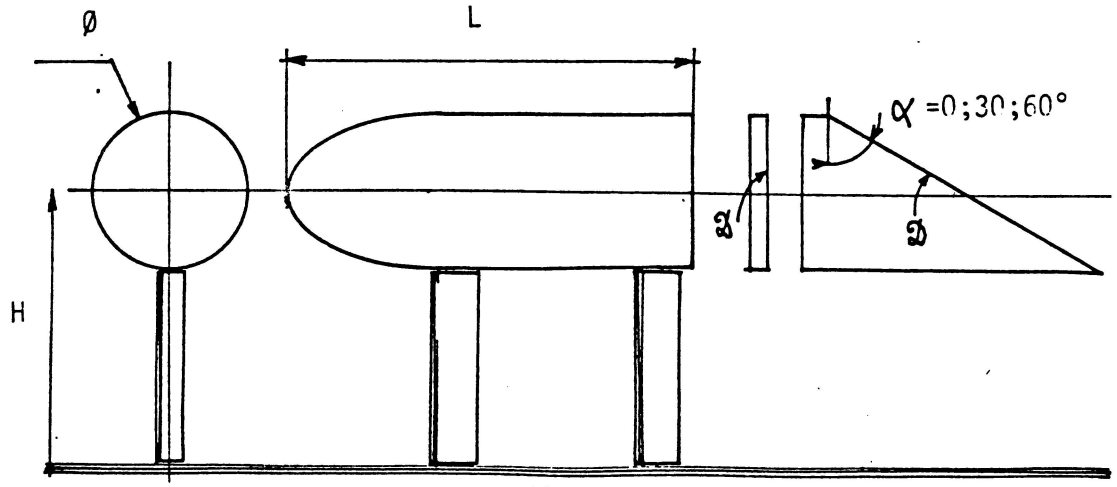

figure 1.1

*Numbers in the margin indicate pagination in the foreign text.

The analysis was based on:

--streamline visualizations using paste
--wake visualizations with bubbles (EMIBUL technique)
--tracings of boundary layer profiles at the base area edge $\mathfrak{B}$ [6].

The results presented here are those for $H/\emptyset = 2$.

The boundary layer readings make possible an approximate calculation of the intensity of the wake vortex emitted at the separation line $\mathfrak{D}$:

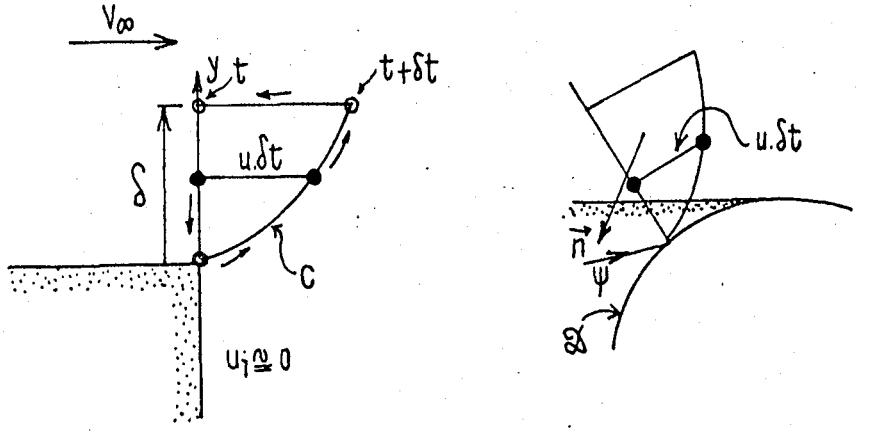

Figure 1.2

The circulation $\delta\Gamma$ on contour C, which is defined in figure 1.2 is, during the period of time δt: /1.2

$$\delta\Gamma = \int_C \vec{V}.d\vec{l} = \iint_S \mathrm{curl}\vec{V}\cdot\vec{n}\,d\sigma \qquad (1.1)$$

If one supposes that the flow is locally two dimensional, one obtains, with:

$$\mathrm{curl}\vec{V}.\vec{n} = \zeta \cong -\frac{\partial u}{\partial y}$$

and

$$dx = u\,dt,$$

$$\frac{1}{V_\infty^2}\frac{d\Gamma}{dt} \cong K V_\infty^2$$

with

$$K = 0.5\left(\frac{u_e}{V_\infty}\right)^2 \qquad (1.2)$$

where u_e is the velocity outside the boundary layer. It has been assumed here that the velocity u_i at the base area is negligible.

1.2 Experimental Results

The observations and photographs reveal the following elements: ($R_L \cong 1.2 \times 10^6$).

1.2.1 $\alpha = 0$

The vorticity discharge emitted by the boundary layer is

constant along the separation line $\mathfrak{D}$ (figure 1.3 and table 1.1, in which the values of u_e/V_∞, δ, and K given by equation (1.2) are noted).

/1.3

Table 1.1

θ	u_e/V_∞	δ(mm)	K
0°	1.03	10	0.53
30°	1.02	10.5	0.52

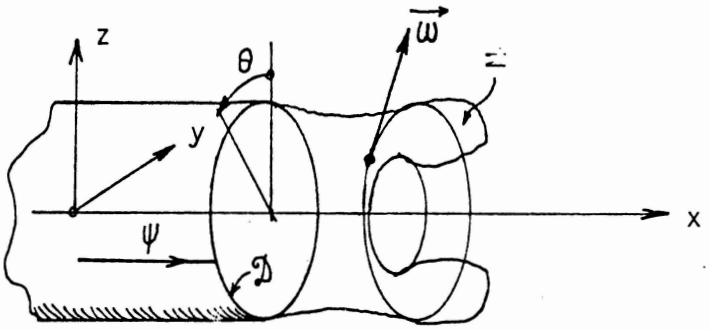

Figure 1.3

The vorticity vector $\vec{\omega}$ associated with each vortex ring is parallel to the yz plane, and the vortex sheet Σ is symmetric about the x-axis. Finally, the streamlines ψ remain parallel to the x-axis and are perpendicular to line $\mathfrak{D}$. The lift $\vec{F}_z$ of such a body when it is located far from the ground is zero and its drag is situated at point a of the curve $C_x = f(\alpha)$ (traced in figure 1.8, which is excerpted from [2]).

1.2.2 $\alpha = 30°$

The streamline visualizations show that the streamlines ψ are perpendicular to the line $\mathfrak{D}$. The slight base area inclination causes dissymmetry in the wake, but its two dimmensional structure is conserved. Representative drag point b in figure 1.8 confirms this.

1.2.3 $\alpha = 60°$

i) The structure of the vortex sheet is greatly modified even though, as shown in photo 1, the streamlines remain perpendicular to $\mathfrak{D}$. (See figure 1.4.)

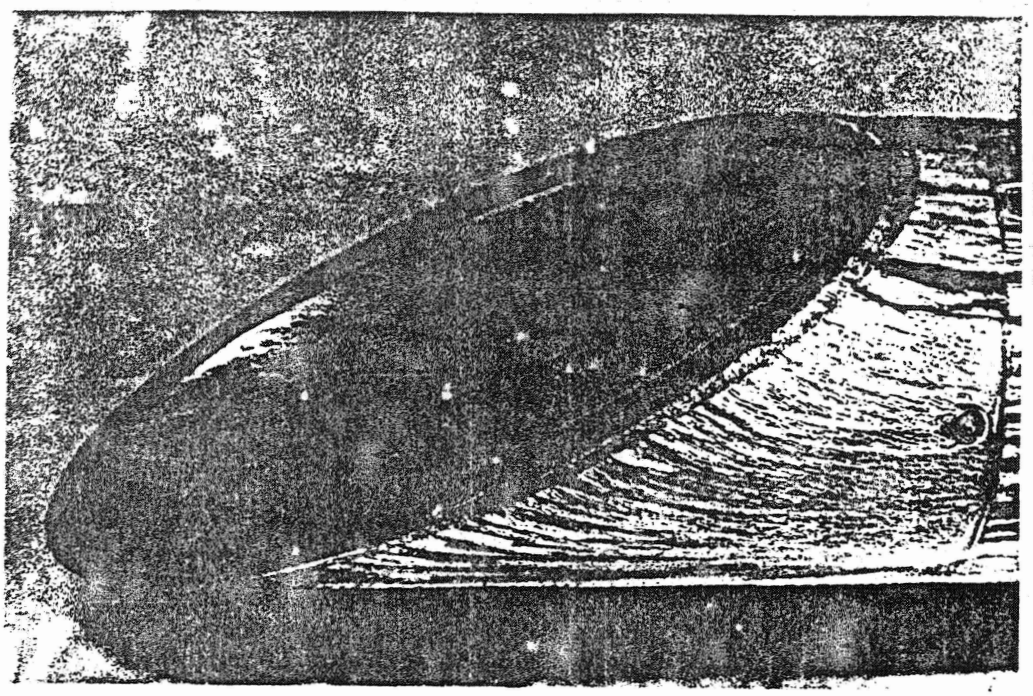

PHOTO 1 $\alpha = 60°$

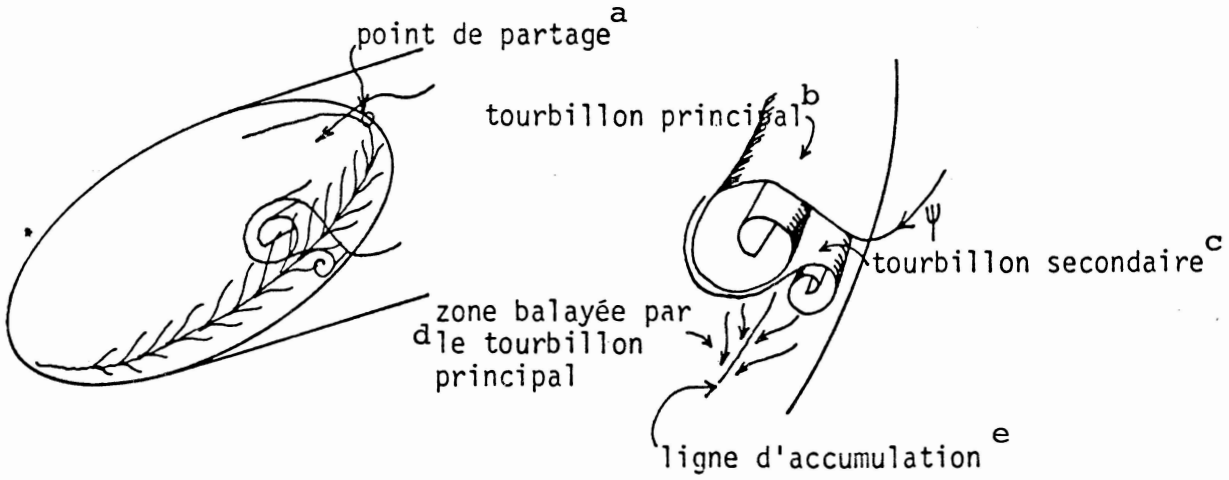

Figure 1.4

Key: a) dividing point
b) main vortex
c) secondary vortex
d) region swept by main vortex
e) accumulation line

Streamline visualizations of the base area reveal secondary rollups similar to those observed in swept wings (Werle [7]). These rollups are illustrated in figure 1.5, which is based on photographs. /1.4

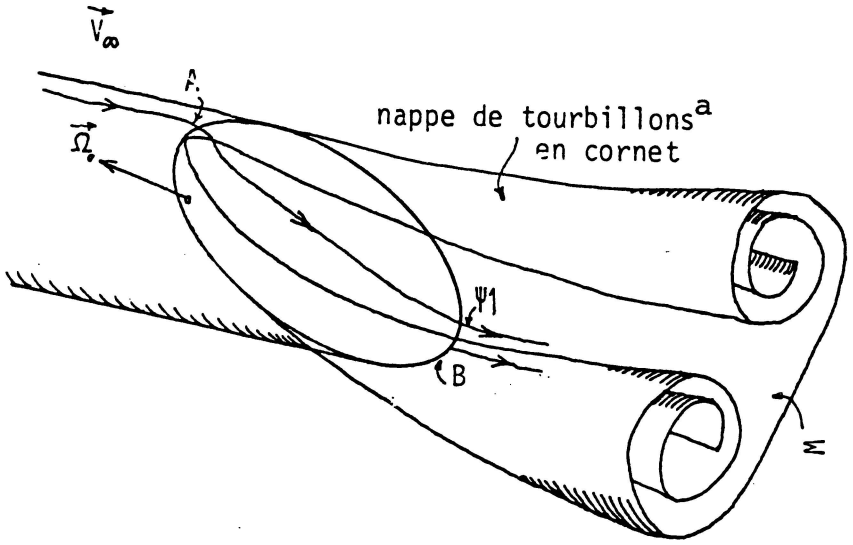

Figure 1.5

Key: a) wake rollup

These observations were recently confirmed by H. Werle through visualizations made in a water tunnel on a body similar to the one described in figure 1.1.

In addition, three-dimensional effects are preponderant. The vortex sheet splits at A in figure 1.5, and a rolled up wake is emitted all along contour $\mathfrak{D}$.

In order to satisfy this scheme, it is necessary that the vorticity vector $\vec{\omega}$ emitted be tangent at B to line $\mathfrak{D}$ and evolve continually from B towards A in such a way that it is practically parallel to $\vec{V}_\infty$ at A.

ii) The photographic data obtained with the bubble technique (see photos 2 and 3) clearly show the formation of the two lateral vortices. The flow remains separated in the median plane of the /1.5

base area, probably with the formation of a bulb at A, as the downstream point B behaves like the following edge of a wing.

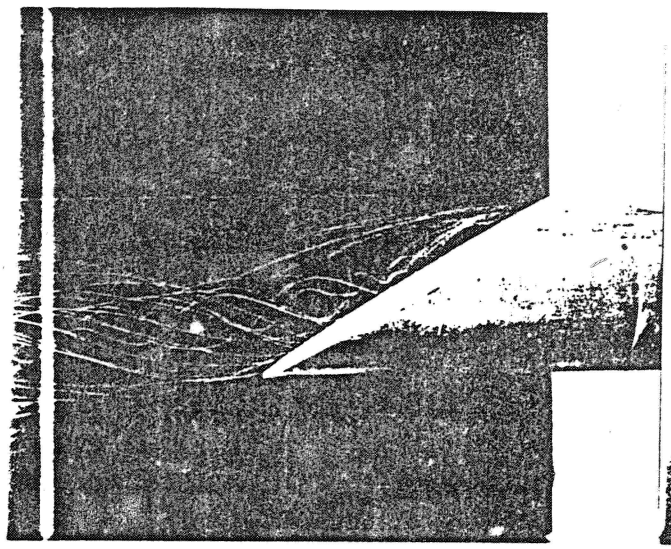

PHOTO 2

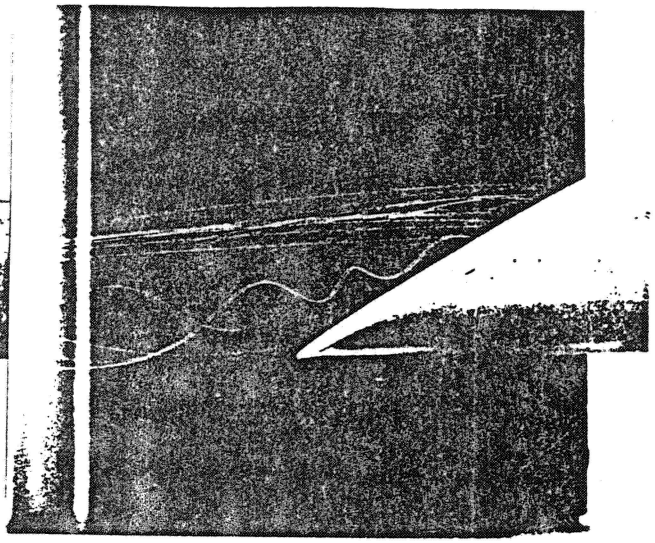

PHOTO 3

iii) This last remark is confirmed by the readings of static pressure on the wall at the median line (figure 1.6). The high pressure in the downstream region shows that the extrados streamline Ψ_1 is strongly deflected in the direction of $\vec{V}_\infty$ by the intrados flow. (See also figure 1.9, which was taken from [2].)

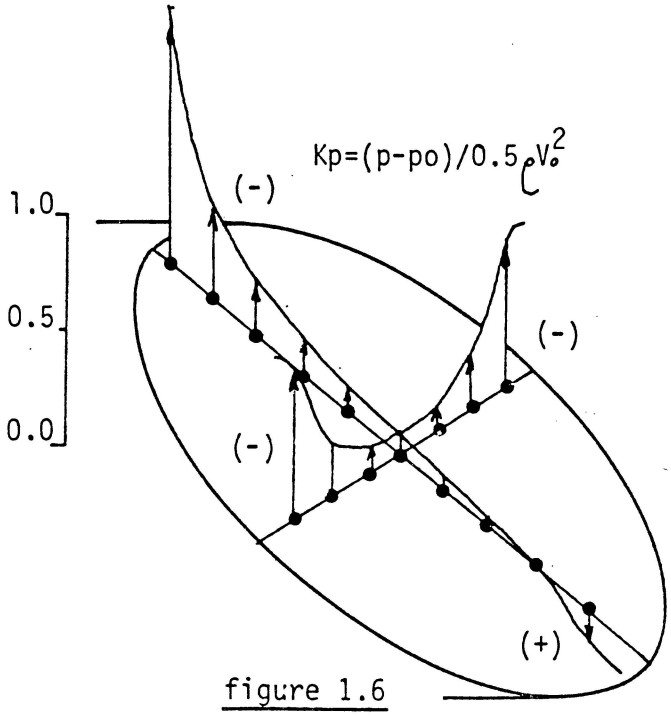

figure 1.6

iv) The boundary layer readings along contour $\mathcal{D}$ have made it possible to calculate the evolution of the parameter K, equation (1.2), as a function of the angular positions θ (figure 1.7). /1.6

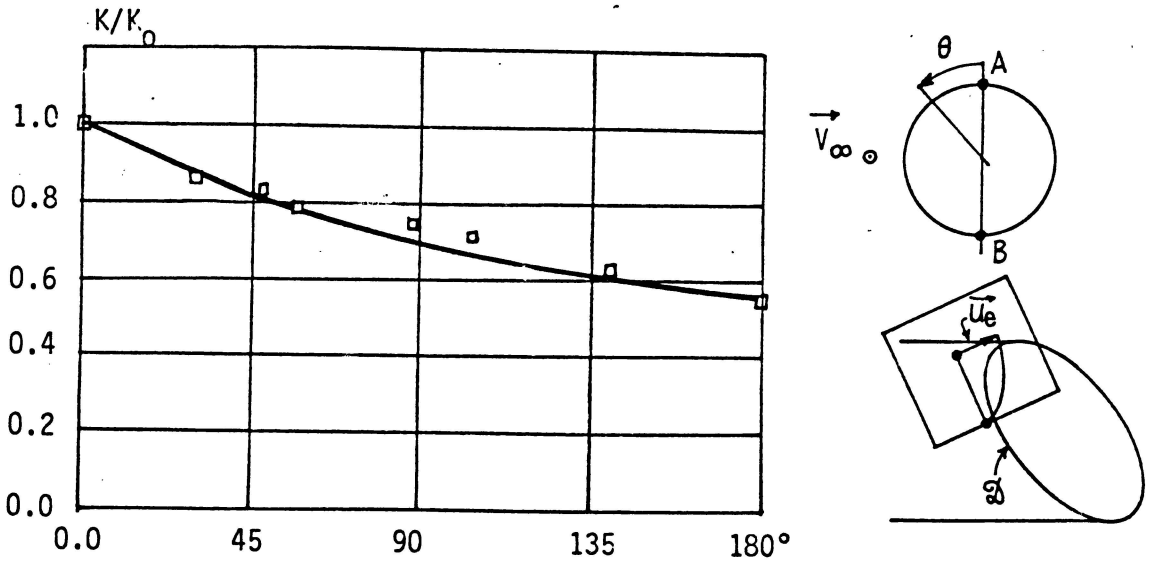

figure 1.7

The readings were made by finding the direction of the velocity vector $\vec{u}_e$. The velocities were then measured in a plane perpendicular to the wall.

/1.7

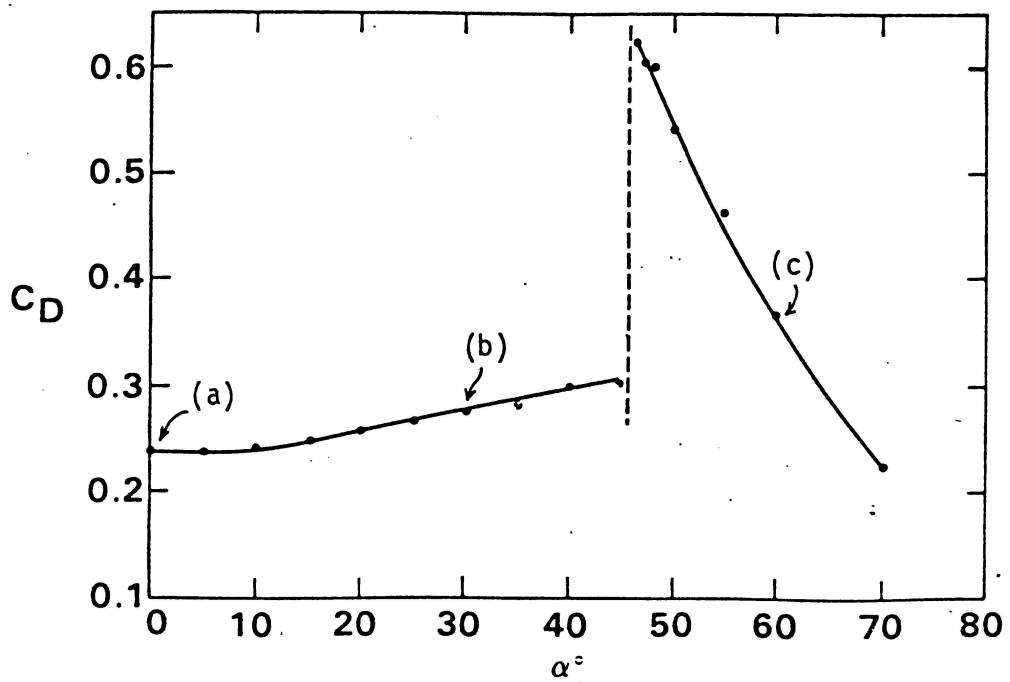

figure 1.8

excerpted from [2] , T. MOREL.

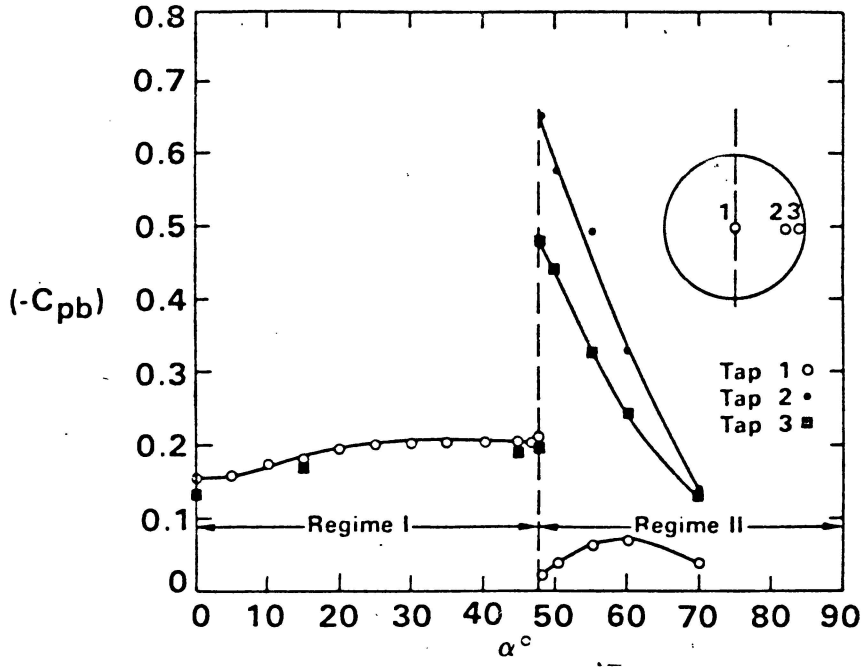

figure 1.9

excerpted from [2], T. MOREL

Chapter 2: Theoretical Basis

2.1 The Problem

It is proposed to solve the following problem, representing the flow of an incompressible, inviscid fluid, defined by the equations [4]:

$$\frac{\partial \vec{V}}{\partial t} - \vec{V} \times \nabla \times \vec{V} = -\overrightarrow{\text{grad}}\left(\frac{p}{\rho} + \frac{1}{2}V^2\right) \tag{2.1}$$

$$\text{div}\,\vec{V} = 0 \tag{2.2}$$

and the boundary conditions:

$$\vec{V}.\vec{n}\,\big|_S = 0 \tag{2.3}$$

$$\vec{V} \to \vec{V}_\infty \quad , (x^2+y^2+z^2) \to \infty \tag{2.4}$$

$\vec{V}$ in the equations designates the velocity vector, p is the pressure, and ρ the mass density. The slip condition (2.3) is applied to solid obstacles inside an unbounded domain with uniform

velocity $\vec{V}_\infty$ at infinity.

By taking the curl of (2.1) so as to intorduce the vector $\vec{\omega}$ = curl $\vec{V}$, the preceding system can be written in the purely kinematic form:

$$\left.\begin{aligned}&\frac{d\vec{\omega}}{dt} = (\vec{\omega}, \operatorname{grad})\vec{V}\\ &\operatorname{div}\vec{V} = 0\end{aligned}\right\} \tag{2.5}$$

where

$$\frac{d\vec{\omega}}{dt} = \frac{\partial\vec{\omega}}{\partial t} + (\vec{V}.\operatorname{grad})\vec{\omega} \tag{2.6}$$

designates the particle derivative in Helmholtz's equation (2.5).

2.2 Calculation of the Velocity Field

/2.2

In the problem (2.5), (2.6) with boundary conditions (2.3) and (2.4), the velocity field $\vec{V}$ can be represented by Green's function [9, 1]:

$$\begin{aligned}&\iiint_v \vec{\omega}_Q \times \overrightarrow{\operatorname{grad}}\left(\frac{1}{r}\right)d\nu_Q + \iiint_v \operatorname{div}\vec{V}_Q . \overrightarrow{\operatorname{grad}}\left(\frac{1}{r}\right)d\nu_Q\\ &- \iint_S (\vec{n}.\vec{V})_Q \overrightarrow{\operatorname{grad}}\left(\frac{1}{r}\right)d\sigma_Q - \iint_S (\vec{n}\times\vec{V})_Q \times \overrightarrow{\operatorname{grad}}\left(\frac{1}{r}\right)d\sigma_Q\\ &= -\iiint_v \vec{V}_Q . \Delta\left(\frac{1}{r}\right)d\nu_Q .\\ &r = |\vec{X}_Q - \vec{X}_P| .\end{aligned} \tag{2.7}$$

This function gives an expression for $\vec{V}$ at any point P of a volume v inside a closed surface S whose normal $\vec{n}$ points inward.

When point P belongs to volume v, the second member of (2.7) has the value $4\pi\vec{V}_P$.

It is equal to zero when P is outside volume v.

Let there be two concentric surfaces S_0 and S_1 (figure 2.1).

Let V_1 be the volume between S_o and S_1 and v_2 be the volume inside S_1.

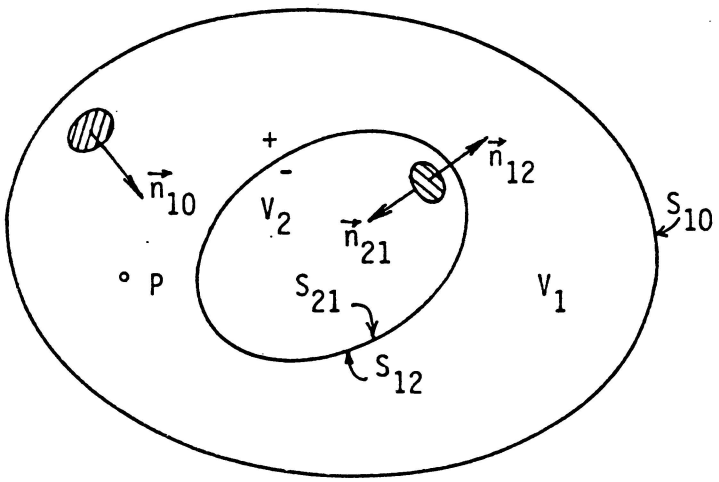

figure 2.1

2.2.1 /2.3

Equation (2.7) written for a point P inside volume v_1 is:

$$\iiint_{v_1} \vec{\omega}_1 \times \overrightarrow{\text{grad}}\left(\frac{1}{r}\right) dv_Q + \iiint_{v_1} \text{div}\vec{V}_1 \cdot \overrightarrow{\text{grad}}\left(\frac{1}{r}\right) dv_Q$$

$$- \iint_{S12} (\vec{n} \times \vec{V}) \times \overrightarrow{\text{grad}}\left(\frac{1}{r}\right) d\sigma_Q - \iint_{S12} (\vec{n} \cdot \vec{V}) \cdot \overrightarrow{\text{grad}}\left(\frac{1}{r}\right) d\sigma_Q$$

$$- \iint_{S10} (\vec{n} \times \vec{V}) \times \overrightarrow{\text{grad}}\left(\frac{1}{r}\right) d\sigma_Q - \iint_{S10} (\vec{n} \cdot \vec{V}) \cdot \overrightarrow{\text{grad}}\left(\frac{1}{r}\right) d\sigma_Q = 4\pi \vec{V}_p \qquad (2.8)$$

2.2.2

Since the surface S_{10} is that of a sphere whose radius $R \to \infty$, equation (2.7) together with condition (2.4) yields for a point within S_{10}:

$$- \iint_{S10} (\vec{n} \times \vec{V}) \times \overrightarrow{\text{grad}}\left(\frac{1}{r}\right) d\sigma_Q - \iint_{S10} (\vec{n} \cdot \vec{V}) \cdot \overrightarrow{\text{grad}}\left(\frac{1}{r}\right) d\sigma_Q = 4\pi \vec{V}_\infty$$

and relation (2.8) becomes:

$$4\pi\vec{V}_P = 4\pi\vec{V}_\infty + \iiint_{v_1} \vec{\omega}_1 \times \overrightarrow{\text{grad}}\left(\frac{1}{r}\right) dv_Q + \iiint_{v_1} \text{div}\,\vec{V}_1 \cdot \text{grad}\left(\frac{1}{r}\right) dv_Q$$
$$- \iint_{S_{12}} (\vec{n} \times \vec{V}) \times \overrightarrow{\text{grad}}\left(\frac{1}{r}\right) d\sigma_Q - \iint_{S_{12}} (\vec{n} \cdot \vec{V}) \cdot \overrightarrow{\text{grad}}\left(\frac{1}{r}\right) d\sigma_Q \qquad (2.9)$$

2.2.3

It is interesting to find any possible discontinuities in velocity across S_{12}. To do this, (2.7) is written for P outside volume v_2:

$$\iiint_{v_2} \vec{\omega}_2 \times \overrightarrow{\text{grad}}\left(\frac{1}{r}\right) dv_Q + \iiint_{v_2} \text{div}\,\vec{V}_2 \cdot \overrightarrow{\text{grad}}\left(\frac{1}{r}\right) dv_Q$$
$$- \iint_{S_{21}} (\vec{n} \times \vec{V}) \times \overrightarrow{\text{grad}}\left(\frac{1}{r}\right) d\sigma_Q - \iint_{S_{21}} (\vec{n} \cdot \vec{V}) \cdot \text{grad}\left(\frac{1}{r}\right) d\sigma_Q = 0 \qquad (2.10)$$

If it is assumed that, in volume v_2:

$$\text{div}\,\vec{V}_2 = 0$$
$$\vec{\omega}_2 = 0 \qquad (2.11)$$

Adding (2.9) to (2.10) while including the boundary condition (2.2) results in: /2.4

$$4\pi\vec{V}_P = 4\pi\vec{V}_\infty + \iiint_{v} \vec{\omega} \times \overrightarrow{\text{grad}}\left(\frac{1}{r}\right) dv_Q \qquad \text{(a)}$$
$$- \iint_{S} [(\vec{n}^+ \times \vec{V}^+) + (\vec{n}^- \times \vec{V}^-)] \times \overrightarrow{\text{grad}}\left(\frac{1}{r}\right) d\sigma_Q \qquad \text{(b)} \quad (2.12)$$
$$- \iint_{S} [(\vec{n}^+ \cdot \vec{V}^+) + (\vec{n}^- \cdot \vec{V}^-)] \cdot \overrightarrow{\text{grad}}\left(\frac{1}{r}\right) d\sigma_Q \qquad \text{(c)}$$

where (+) and (-) have replaced subscripts (12) and (21).

The integral equation (2.12) can be considered as the basis of the method of singular points. The problem posed by (2.5) and (2.6) and the boundary conditions (2.3) and (2.4) are replaced by (2.5), (2.12), and condition (2.3) on S.

2.2.4 Method of Singular Points

i) Integral (a) of equation (2.12) expresses the contribution at P of all vorticity vectors $\vec{\omega}$ contained in volume v_1. It should be noted that the volume integral only covers the regions of v_1 where $\vec{\omega}$ does not equal zero. This makes its calculation easy when the domain v is unlimited.

In addition [1], as the fluid is assumed to be incompressible, the calculations are carried out for the vector:

$$\vec{\Omega} = \vec{\omega}\delta v \tag{2.13}$$

where $\vec{\omega}$ represents the average vortex intensity associated with the particle of constant volume δv .

ii) Integral (b) can be written, with $\vec{n}^+ = -\vec{n}^- = \vec{n}$:

$$-\iint_S \vec{n}\left(\vec{V}^+ - \vec{V}^-\right)\overrightarrow{\text{grad}}\left(\frac{1}{r}\right)d\sigma_Q \tag{2.14}$$

The local scalar quantity $q = \vec{n}\cdot(\vec{v}^+ - \vec{v}^-)$ is equal to the increase in the normal component of velocity across the surface element $d\sigma_Q$ and therefore has the dimensions of a rate per unit area.

The contribution of velocity corresponding to integral (b) is then

$$4\pi\vec{V}_{p_q} = \iint_S -q\cdot\overrightarrow{\text{grad}}\left(\frac{1}{r}\right)d\sigma_Q \tag{2.15}$$

When point P approaches point Q (figure 2.2), the contribution /2.5 of the integral at the singularity is $2\pi q_p\vec{n}^+$ on the n^+ side and $2\pi q_p\vec{n}^- = -2\pi q_p\vec{n}^+$ on the n^- side, with the increase $\vec{n}\cdot(\vec{v}^+ - \vec{v}^-)$ equal to the local intensity q.

iii) Integral (c) of (2.12) can also be written:

$$-\iint_S \vec{n}\times\left(\vec{V}^+ - \vec{V}^-\right)\times\overrightarrow{\text{grad}}\left(\frac{1}{r}\right)d\sigma_Q \tag{2.16}$$

and the local vectoral quantity $\vec{\gamma} = \vec{n}\times(\vec{v}^+ - \vec{v}^-)$ is equal to the

surface vortex density associated with the discontinuity in tangential velocity across surface S.

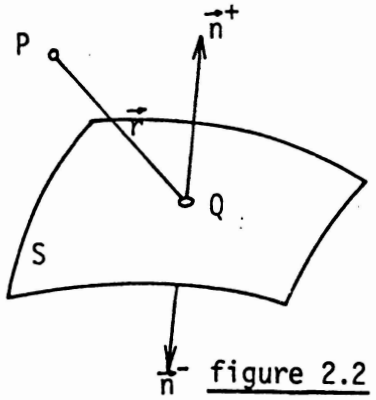

figure 2.2

The contribution of velocity corresponding to integral (c) is:

$$4\pi\vec{V}_{P\gamma} = \iint_S -\vec{\gamma} \times \overrightarrow{\text{grad}}\left(\frac{1}{r}\right) d\sigma_Q \qquad (2.17)$$

This is the classic Biot-Savart equation [10]. The integral's contribution at the singularity is $2\pi\vec{\gamma}x\vec{n}^+$ on the n^+ side and $2\pi\vec{\gamma}\ x\vec{n}^- = -2\pi\vec{\gamma}x\vec{n}^+$ on the n^- side, with the increase in the tangential component of velocity equal to $\vec{\gamma}x\vec{n}$.

2.2.5 Application to Physical Problems

The integral equation (2.12) is written:

$$4\pi\vec{V}_P = 4\pi\vec{V}_\infty + \iiint_V \vec{\omega} \times \overrightarrow{\text{grad}}\left(\frac{1}{r}\right) dv_Q \qquad \text{(a)}$$

$$- \iint_S q \cdot \overrightarrow{\text{grad}}\left(\frac{1}{r}\right) d\sigma_Q \qquad \text{(b)} \qquad (2.18)$$

$$- \iint_S \vec{\gamma} \times \overrightarrow{\text{grad}}\left(\frac{1}{r}\right) d\sigma_Q \qquad \text{(c)}$$

i) The hypothesis of continuity of tangential velocity on S, or /2.6

$$\vec{n}^+ x \vec{V}^+ = -\vec{n}^- x \vec{V}^-$$

leads to the "source" solution. It is known that this solution is particularly well adapted to external zero-lift Neumann problems. In contrast, the distribution of sources giving an imposed distribution of normal velocity $\vec{V}\cdot\vec{n}$ on an internal surface S (internal Neumann problem), is generally not unique. (Hunt [5]).

ii) The hypothesis of continuity for normal velocity on S, $n^+\cdot V^+ = n^-\cdot V^-$, leads to the "vortex" solution.

This solution is suitable for problems with positive lift and makes it possible to take into account vortex sheets for incompressible flows of transient viscosity. The vortex intensities in the sheet are then directly derived from the intensities $\vec{\gamma}$ on the surface of the body (Rehbach [1]).

Let a volume element [11]

$$d\nu_Q = \varepsilon d\sigma_Q$$

and $\vec{\omega}$ be the vorticity vector at a point Q or a surface S (figure 2.3). The quantity ε can represent the local thickness of the boundary layer and $\vec{\omega}$ the transported viscosity vector.

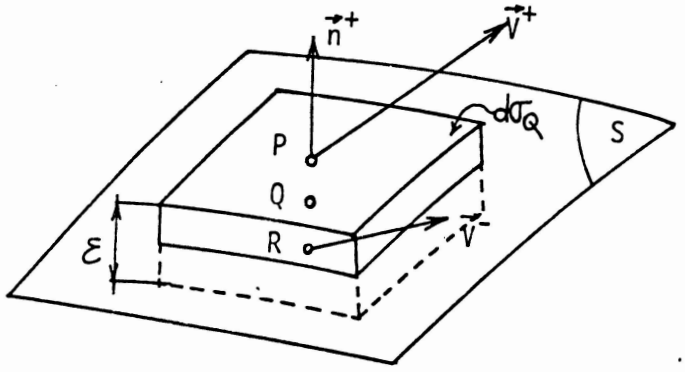

figure 2.3

The application of Guass's theorem to infinetesimal cylindrical volume element $d\nu$ yields the following approximate result:

$$\vec{\omega}\varepsilon d\sigma = (\vec{n}^+ \times \vec{V}^+ + \vec{n}^- \times \vec{V}^-) d\sigma + \iint_{\text{lateral surface}} \tag{2.19}$$

or $$\vec{\omega}\varepsilon d\sigma = \vec{n} \times (\vec{V}^+ - \vec{V}^-) d\sigma + \iint_{\text{lateral surface}}$$

Note that $$\vec{\gamma} = \vec{\omega}\varepsilon$$

By making $\varepsilon \to 0$ (Reynolds $\to \infty$) in such a way that the product /2.7
$\vec{\omega}\varepsilon$ remains constant, equation (2.19) yields:

$$\vec{\gamma} = \vec{n} \times (\vec{V}^+ - \vec{V}^-) \tag{2.20}$$

which is the vectorial quantity already obtained in paragraph 2.23 with Green's function.

Finally, (figure 2.4) if surface S is a closed surface on which the restriction $\delta\phi/\delta n = 0$ ($\vec{V}^+ \cdot \vec{n}^+ = 0$) everywhere is imposed, and if the problem is resolved with the vortex solution, equation (2.19) shows that $\delta\phi^+/\delta n = 0$. It can be deduced from this that the potential within the interior volume is constant and that $\vec{V}^- = 0$ everywhere [5].

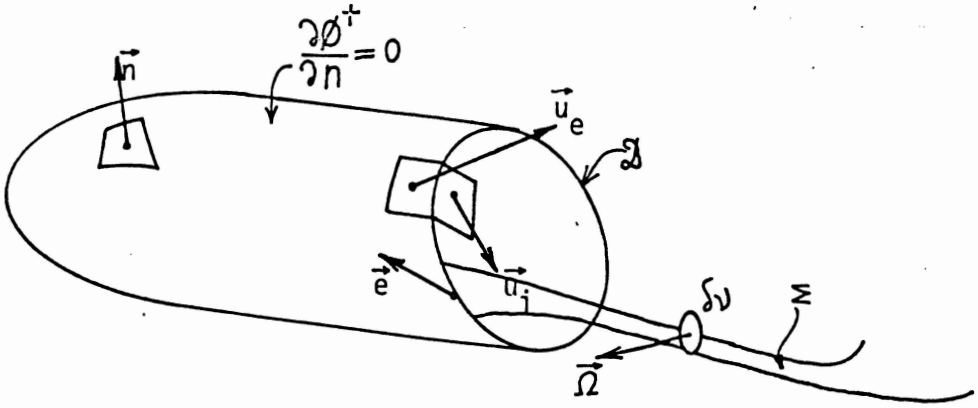

figure 2.4

The local intensity $\vec{\gamma} = \vec{n} \times \vec{V}^+$ therefore is the image of the discontinuity of tangential velocity on surface S when the Reynolds number approaches infinity.

In these conditions the intensities $\vec{\Omega}$ of the vortex particles

which we used to model the wake Σ (figure 2.4) and are followed with the aid of Helmholtz's Equation (2.5) can be determined directly with the aid of the vortex intensities $\vec{\gamma}$ on surface S along the separation line $\mathfrak{D}$.

iii) In contrast, it is not necessary to include the idea of an infinite Reynolds number for the source solution. /2.8

The vorticity discharge into the wake can in principle be calculated on the basis of physical data valid for a fixed Reynolds number.

Three-dimensional emission models do not seem to exist at present. Approximate schemes based on local two-dimensional approaches are used, and the vorticity discharge has the form (1.2):

$$\frac{\delta \vec{\Omega}}{\delta t} = k \cdot 0{,}5 \cdot \left(u_e^2 \pm u_i^2\right) \cdot \vec{e} \qquad (2.21)$$

In equation (2.21) u_e and u_i represent the velocities on either side of $\mathfrak{D}$ (figure 2.4); k is uniform at a given distance, see [12] and [1]. The main difficulty in the use of this model is in the choice of the unit vector $\vec{e}$, whose direction is closely linked to the extent of the flow's three-dimensional character at the base area.

Thus, for an upright base area, $\vec{\Omega}$ is everywhere tangent to the separation line, whereas for a highly inclined base area, the vector $\vec{\Omega}$ varies continuously along $\mathfrak{D}$.

This point is numerically analyzed in the following chapter.

2.3 Calculation of Pressure

The pressure field is related to the velocity field by equation (2.1), which, in the regions where curl $\vec{V} = 0$, i.e. outside the vortex sheets, is written:

$$p + \frac{1}{2}\rho V^2 - \frac{\partial \Phi}{\partial t} = C(t) \qquad (2.22)$$

where $\vec{V} = \overrightarrow{\text{grad}}\ \emptyset$ and C(t) is a constant function of time t.

It will be assumed in the following discussion that a steady state on surface S has been achieved and that the potential $\emptyset$ tends toward a finite limit, which is physically likely.

2.3.1 Upright Base Area /2.9

Let there be a cylindrical body whose axis is directed along the vector and which possesses an upright base area.

Physical observations (Werle [7], Siriex [16]) show that downstream from the base area there is a vortical recirculation region R2 (figure 2.5a) separated from region R1 by streamline C.

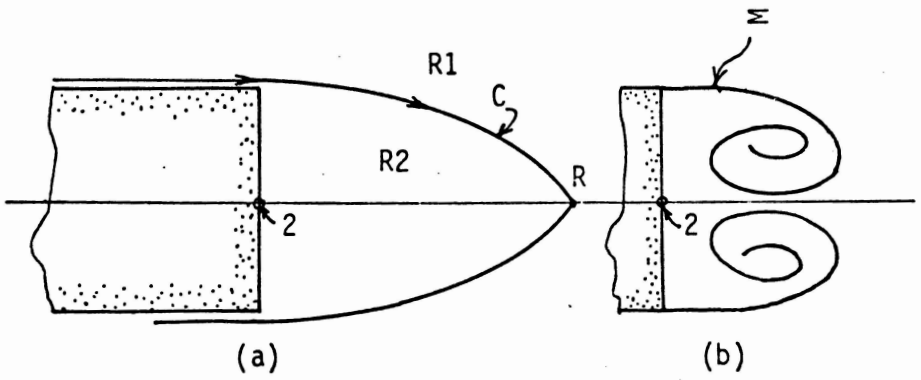

figure 2.5

Point R is a free reattachment point.

It is known in addition that physically and for Reynolds numbers on the order of 10^6, the velocity at the base area is small. The pressure coefficients, reduced to p_∞ and $[V_\infty]$, are on the order of -0.2 at the axis. This value remains practically constant over the base area, but depends on the configuration of the edge.

The constants C_1 and C_2 in regions R1 and R2 are therefore different, and for points 1 and 2 located in the two regions:

$$p_1 + \frac{1}{2}\rho V_1^2 = p_\infty + \frac{1}{2}\rho V_\infty^2 = p_{i1}$$

$$p_2 + \frac{1}{2}\rho V_2^2 = p_{i2}$$

If one examines a point 2 on the base area where $V_2 = 0$ and a point 1 in R1 where $V_1 = 0$ also, one will therefore have: /2.10

$$\frac{p_2 - p_1}{\frac{1}{2}\rho V_\infty^2} = \frac{p_{i2} - p_{i1}}{\frac{1}{2}\rho V_\infty^2}$$

or

$$\Delta Kp = \frac{\Delta p_i}{\frac{1}{2}\rho V_\infty^2}$$

The quantity ΔKp is the irreversible energy loss due to viscous effects. This loss is not taken into account in a perfect fluid model leading to the result in figure 2.5b. It therefore seems difficult to obtain realistic base area pressure coefficients in this case. (See also [13], p. 14.)

2.3.2 Inclined Base Area ($\alpha = 60°$)

In cases in which the sheet is split, the problem is different. For points on the base area which are not located near the separation line $\mathfrak{D}$, there is a steady-state streamline in which (figure 2.6):

$$C_1 = p_\infty + \frac{1}{2}\rho V_\infty^2 = p + \frac{1}{2}\rho V^2 \qquad (2.23)$$

The pressure coefficients can then be calculated by:

$$Kp = 1 - \left(\frac{V}{V_\infty}\right)^2 \qquad (2.24)$$

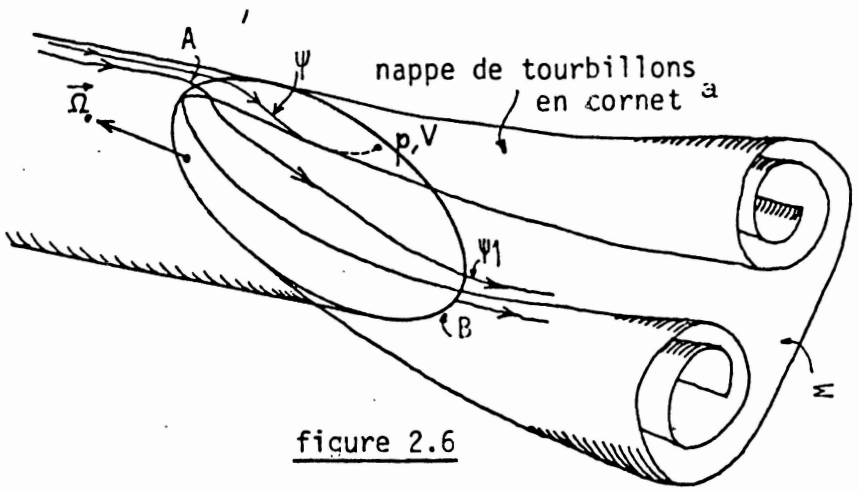

figure 2.6

Key: a) vortex wake rollup

2.4 Calculation of Stress /2.11

2.4.1

When a velocity-pressure relation can be defined for all points in S, the aerodynamic force can of course by calculated by:

$$\vec{F} = \iint_S -p_Q \cdot \vec{n}_Q \cdot d\sigma_Q \qquad (2.25)$$

2.4.2

Referring to equation (2.23), equation 2.24 becomes:

$$\vec{F} = \frac{1}{2}\rho \iint_S V_Q^2 \cdot \vec{n}_Q d\sigma_Q \qquad (2.26)$$

In the vortex solution equation (2.26) (Milne-Thomson [11], pp 185-86) becomes:

$$\vec{F} = \rho \iint_S \vec{V}_Q \times \vec{\gamma}_Q d\sigma_Q \qquad (2.27)$$

The velocity vector $\vec{V}_Q$ can be decomposed into:

$$\vec{V}_Q = \vec{V}_\infty + \vec{V}_{\gamma Q} + \vec{V}_{\omega Q}$$

where $\vec{V}_{\gamma Q}$ and $\vec{V}_{\omega Q}$ respectively represent the velocities induced in Q by the vortex layer $\vec{\gamma}$ distributed on S and by the point singularities contained in the sheet Σ.

The aerodynamic force $\vec{F}$ is then:

$$\vec{F} = \vec{F}_0 + \vec{F}_1 + \vec{F}_2$$

with

$$\begin{aligned} \vec{F}_0 &= \rho \vec{V}_\infty \times \iint_S \vec{\gamma}_Q \, d\sigma_Q \\ \vec{F}_1 &= \rho \iint_S \vec{V}_{\omega Q} \times \vec{\gamma}_Q \, d\sigma_Q \\ \vec{F}_2 &= \rho \iint_S \vec{V}_{\gamma Q} \times \vec{\gamma}_Q \, d\sigma_Q \end{aligned} \qquad (2.28)$$

In $\vec{F}_0$ and $\vec{F}_1$ the conventional forms of induced lift and drag can be recognized.

Chapter 3: Numerical Results /3.1

3.1 Introduction

The different calculation programs developed on the basis of the preceding theoretical elements have made it possible to numerically study three-dimensional separated flow around cylinders with flat base areas inclined at an angle α (figure 3.1).

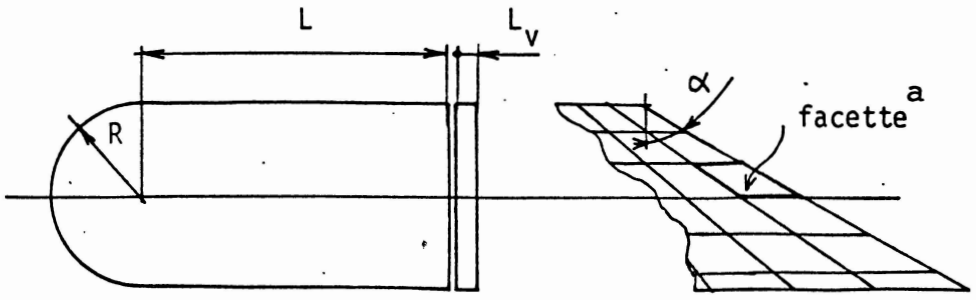

figure 3.1

Key: a) panel

The bodies are broken up into discrete quadrilateral panels. The control point for each of the panels is its center of gravity.

The calculations presented here were carried out for bodies at zero incidence and sideslip located at a great distance from the ground, and with L/R = 3.

The evolution of the vortex particles emitted at the separation contour D is calculated on the basis of Helmholtz's equation (2.5), which for nondimensional variables is written:

$$\vec{\bar{\omega}} = \frac{\vec{\omega} l}{V_\infty} \quad , \quad \vec{\bar{V}} = \frac{\vec{V}}{V_\infty} \quad , \quad \bar{t} = \frac{t}{\Delta t} \quad , \quad \vec{\bar{x}}_i = \frac{\vec{x}_i}{l} \quad :$$

$$S \frac{d\vec{\bar{\omega}}}{d\bar{t}} = \left(\vec{\bar{\omega}} \overrightarrow{\text{grad}}\right)\vec{\bar{V}} \tag{3.1}$$

where $S = l/V_\infty \Delta t$ is the Strouhal number associated with l and V_∞, and the vortex release frequency $n = 1/\Delta t$.

The choice of step Δt in the discrete equation associated with (3.1) determines the Strouhal number of the numerical model. If the length l designates the average characteristic dimension of the panels located at [sic], the value of S corresponding to a satisfactory evolution of the sheet is on the order of one.

3.2 Numerical Results: Vortex Solution /3.2

For this type of numerical model and for the results presented, the emission is made from a flap (figure 3.1a) located directly downstream from $\mathfrak{D}$.

The method for creating the vorticity vector $\vec{\Omega}$ is similar to the one proposed by Rehbach [1] for the study of flat wings of zero thickness. The adaptation to three dimensions is sketched out in figures 3.2a, b, and c.

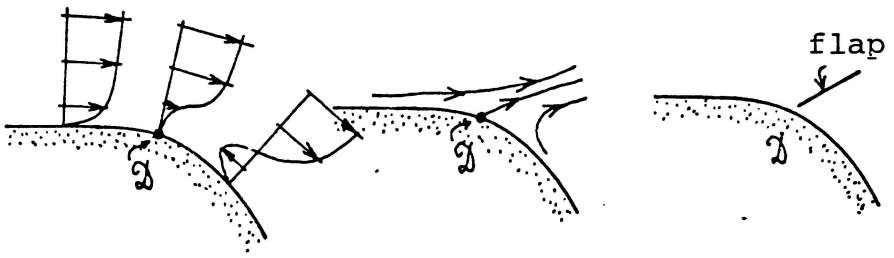

(a) (b) (c)

figure 3.2

The results obtained for α = 0°, 30°, and 60° are traced in figures 3.3, 3.4, and 3.5.

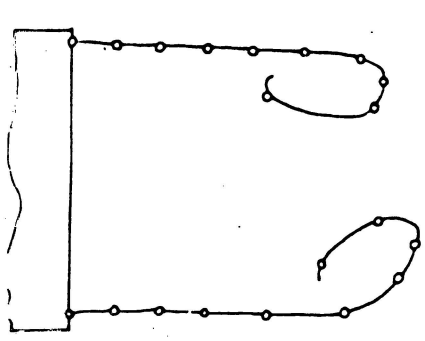

α=0°

figure 3.3

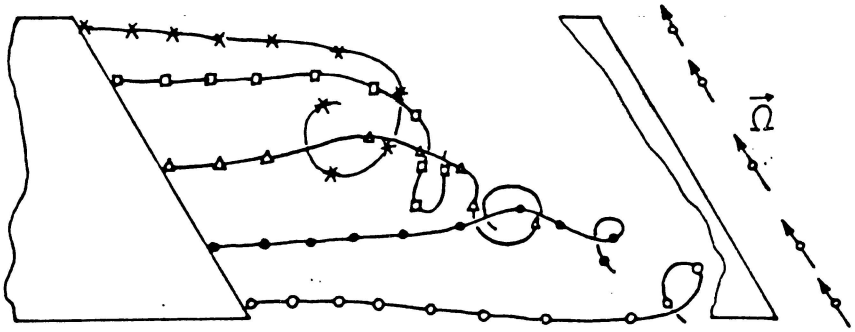

α=30°

Vector $\vec{\Omega}$

figure 3.4

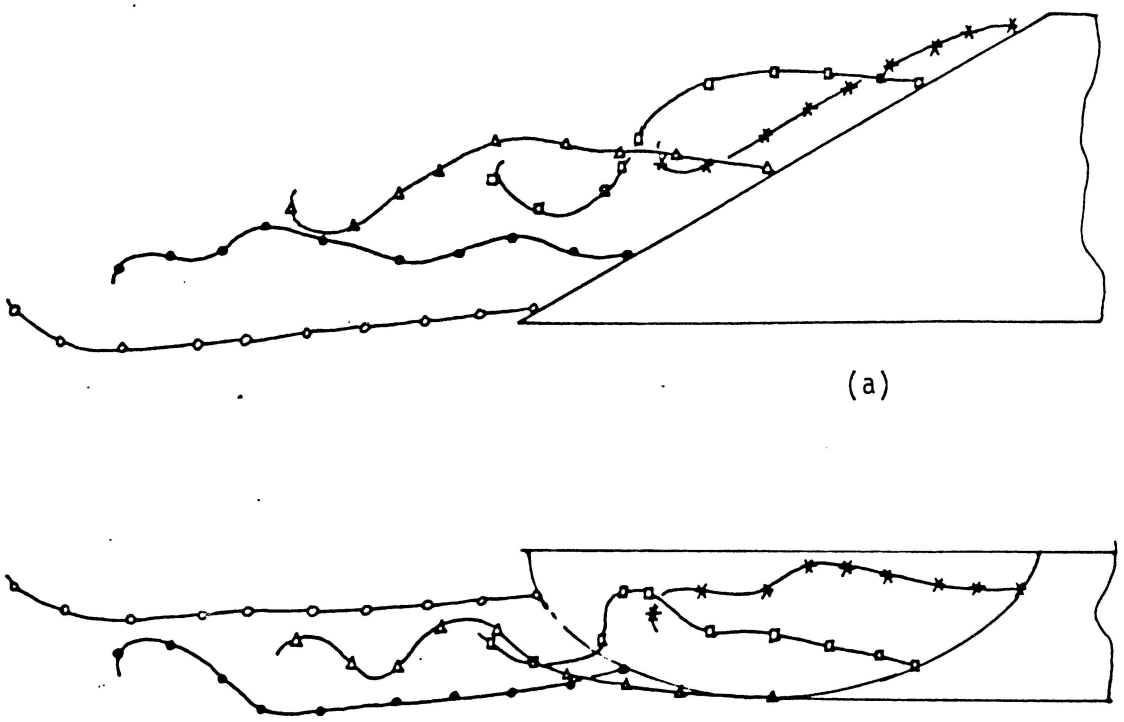

10 step calculation $\alpha = 60°$

figure 3.5

For α = 0° and 30°, the sheet has a two-dimensional separated structure, and the vectors $\vec{\Omega}$ associated with the particles emitted at the flap's following edge remain parallel to $\mathcal{D}$ (figure 3.4b).

Finally, particularly for α = 0°, the velocities on the base area are very small, which is physically correct.

For α = 60°, the emission lines traced on figure 3.5a show lateral rollups beginning to form. The flow is separated on the lower part of the base area and reattached at its upper part, in the median plane.

It should be pointed out that with this model, the emitted vectors $\vec{\Omega}$ remain practically parallel to the following edge of the flaps since the sheet is not split. The direct consequence of this is that the velocities obtained at the base area are insufficient, and

the pressure coefficients remain positive there.

The improvements made recently by Billet [14] in the emission model (elimination of the flap, participation of the panels neighboring $\mathfrak{D}$) should make it possible to obtain good results, while at the same time probably causing the sheet to tear. /3.3

3.3 Numerical Results: Source Solution /3.4

For this type of numerical model, the emission is defined by equation (2.21), with the quantity u_i^2 not being taken into account in the present shceme. The flap associated with the scheme described in paragraph 3.2 is suppressed, and the direction of the vector $\vec{\Omega}$ is arbitrary.

3.3.1

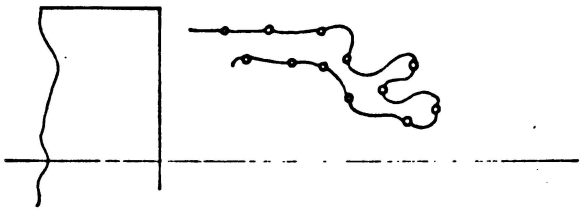

figure 3.6

For $\alpha = 0°$ (figure 3.6), the vector is parallel to [sic]. The result shows a zone of recirculation beginning to form downstream from the base area. The velocities on the base area, reduced to V_∞, are on the order of 0.1, which is physically correct.

3.3.2

For $\alpha = 60°$, several numerical tests are presented. Their goal is to analyze the role of the vectors' direction at emission, whose modulus is defined by equation (2.21):

i) The vector $\vec{\Omega}$ remains parallel to $\mathfrak{D}$: The result in figure 3.7, obtained after an 18-step calculation, confirms the one in figure 3.5. The sheet is not split; the velocities at the base area remain insufficient.

Key: a) numerical instability
b) Vector $\vec{\Omega}$ parallel to contour D
c) 18-step calculation

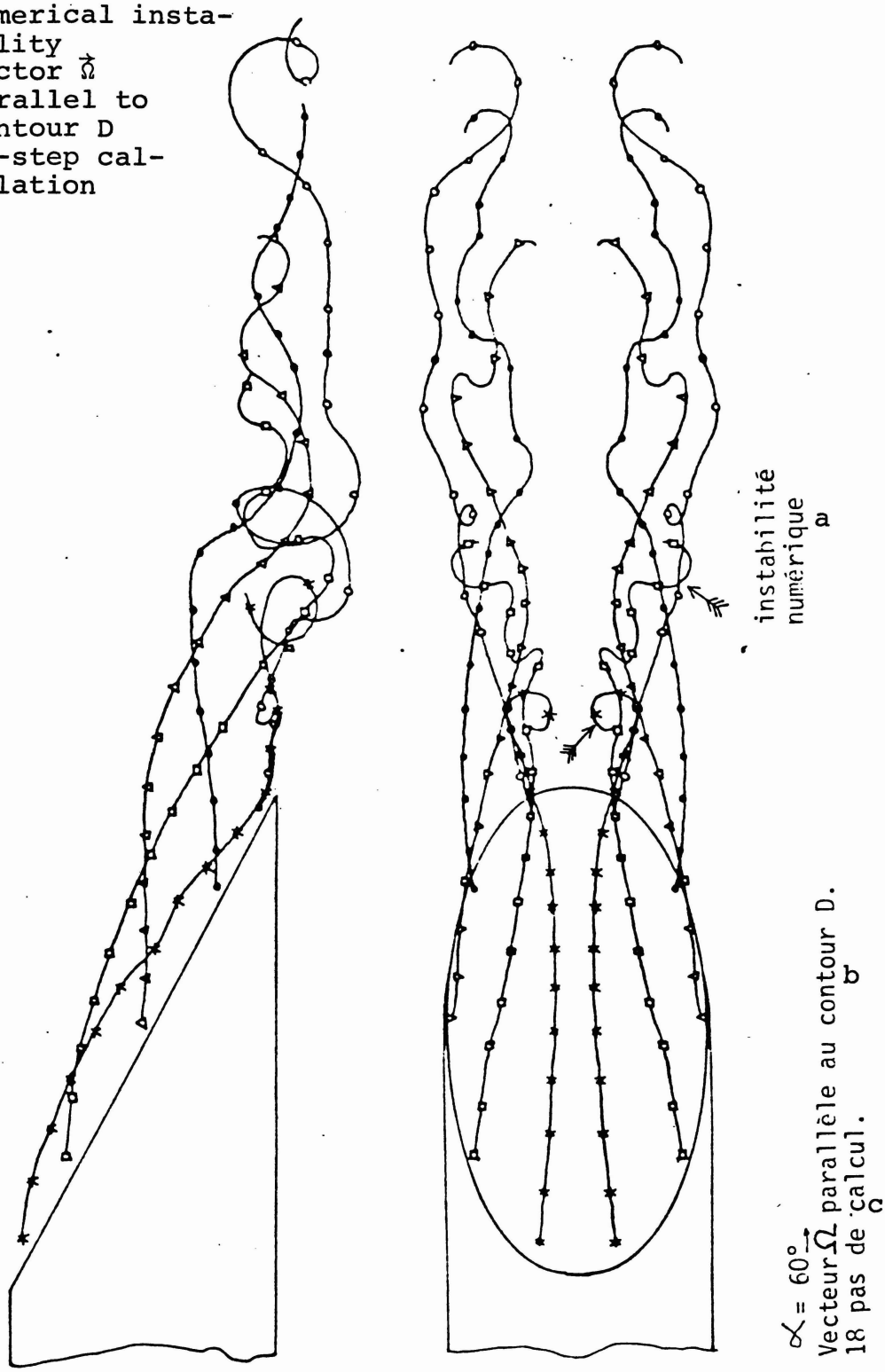

figure 3.7

Key: a) Vector $\vec{\Omega}$ varies along D
b) 18-step calculation

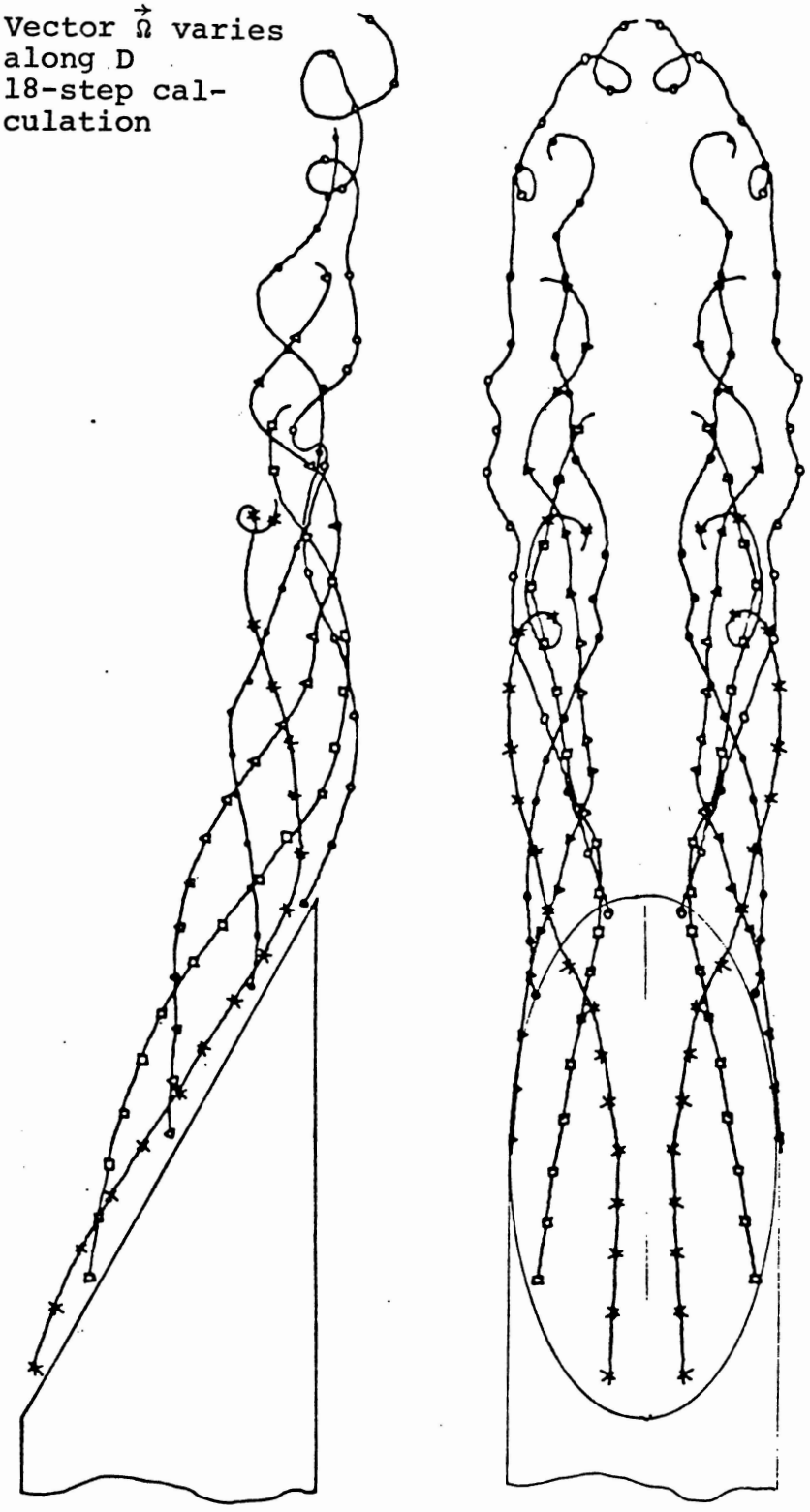

$\alpha = 60°$
Vecteur $\vec{\Omega}$ évolutif le long de D.
18 pas de calcul.
a
b

figure 3.8

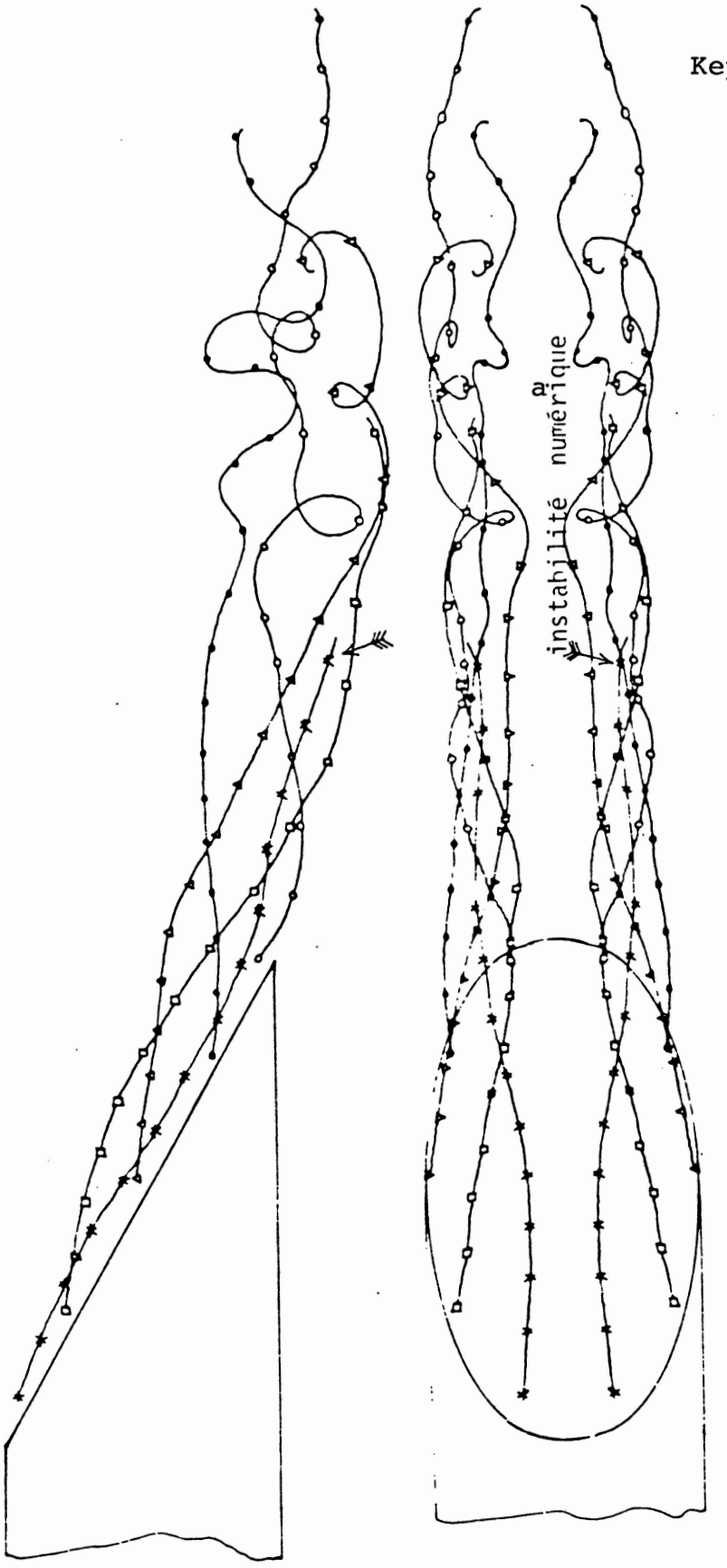

Key: a) numerical instability
b) 18-step calculation

figure 3.9

ii) The vector $\vec{\Omega}$ varies continuously along contour $\mathcal{D}$: The flow is two-dimensional in the downstream part of the base area (figure 3.8). The numerical results obtained are interesting, the sheet is split, and the lateral rollups are satisfactory. The velocities at the base area are greater, but insufficient at $\mathcal{D}$. This is probably due to the fact that the split in the sheet is incomplete, with the emission line (marked with the symbol "*" on figure 3.8) remaining in the median part of the base area.

iii) Since the force exerted on the vector particle $\vec{\Omega}$ has the form $\vec{F} \sim \vec{\Omega} \times \vec{V}$, the sheet is in equilibrium when $\vec{\Omega} \parallel \vec{V}$. For the problem that interests us, the steady state was the only one desired, and it seemed useful to impose these conditions on the emission from the beginning of the calculation.

The results obtained were similar to those analyzed in paragraph ii (figure 3.9) as the velocities at the base area were insufficient. /3.8

It also appeared that the emission line (marked with the symbol "ə"), which was located downstream from the base area, participated in the lateral rollup. This seems to be in contradiction with the experimental measurements, which show that this part of the base area behaves like the following edge of a wing (Chapter 2).

3.4 Conclusion

The body of results presented here shows the possibility of calculating separated flow past thick bodies through the use of a theoretical model based on a discrete wake-vortex representation.

The calculations carried out specify the profound changes in the wake when the base area angle is large.

Our results constitute an as yet incomplete first approximation of the pressure on the base area and show that an in-depth analysis of the mechanism of three-dimensional separation is necessary. This work is in progress.

REFERENCES

[1] Rehbach, C., "Ecoulements avec nappes tourbillonnaires" [Flow with Vortex Sheets], La Recherche Aérospatiale, 5 (1977).

[2] Morel, T., D.J. Maull, and W.H. Hucho, Aerodynamic Drag Mechanisms of Bluff Bodies and Road Vehicles, Plenum Press, 1978.

[3] Milne-Thomson, L.M. Theoretical Hydrodynamics, Macmillan, 1938 and 1950.

[4] Lamb, Sir H., Hydrodynamics, Dover Publications, 1945.

[5] Hunt, B., "The Panel Method for Subsonic Aerodynamic Flows," 1978 lecture series, 4, VKI for Fluid Dynamics, March 1978.

[6] Nodin, F., Projet de fin d'études, Sup. Aéro [Final Degree Project for the Ecole Supérieure de l'Aéronautique], 1979.

[7] Werle, H., "Ecoulements décollés--Etude phénoménologique à partir de visualisations hydrodynamiques" [Separated Flow: Phenomenological Study Based on Flow Visualizations], AGARD Conference Proceedings No. 168, (1975).

[8] Legendre, R., "La condition de Joukowski en écoulement tridimensionnel" [The Joukowski Condition in Three-Dimensional Flow], La Recherche Aerospatiale, 5 (1972), 241-48.

[9] Durand, E., Electrostatique et magnétostatique [Electrostatics and Magnetostatics], Masson et Cie, 1953.

[10] Jacob, C., Introduction mathématique à la Mécanique des Fluides [Mathematical Introduction to Fluid Mechanics], Bucharest, 1959.

[11] Milne-Thomson, L.M., Theoretical Hydrodynamics, 3rd edition, Macmillan, 1952.

[12] Sarpkaya, T. and C.J. Garrison, "Vortex Formation and Resistance in Unsteady Flow," Transactions of the ASME - Journal of Applied Mechanics (March 1963).

[13] Carrière, P., "Notions générales sur les problèmes de confluence" [Some General Comments on Confluence Problems], La Revue Française de Mécanique, 24 (1967).

[14] Billet, Thèse de doctorat, à paraître [Forthcoming doctoral thesis]

[15] Chometon, F. and P. Fontanet, "Etude théorique et expérimentale de l'écoulement bidimensionnel décollé autour d'un profil de véhicule automobile" [Theroetical and Experimental Study of Two-Dimensional Flow Past the Profile of an Automobile], 13th AAAF

Colloquium, Lyons, 1976.

[16] Siriex, M., "Décollement turbulent en écoulement bidimensionnel" [Turbulent Separation in Two-Dimensional Fluid Flow], AGARD Conference Proceedings No. 168, (1975).